International journal of COMADEM
Volume 22 Number 1 January 2019 ISSN 1363-7681

COMADEM

International Journal of Condition Monitoring and Diagnostic Engineering Management

Ruggedized and Improved MEMS-based Sensors for Rolling Stock

James P. Hofmeister, Wyatt Pena, Robert Wagoner, and Douglas L. Goodman[a]

Ridgetop Group, Inc.
3580 West Ina Road
Tucson, AZ 86741
520-742-3300

[a] *+01-520-742-3000*; *goodman@ridgetopgroup.com*

ABSTRACT

This article describes work related to ruggedizing and improving an accelerometer-based sensor, RotoSense™, used for monitoring rolling stock: the locomotives and cars used in trains. A paper, "Accurate Vibration and Speed Measurement on Rotating Shafts using MEMS and IoT Single Wireless Triaxial Sensor," was presented at the 2016 MFPT conference that described a sensor capable of measuring shaft speeds of up to 5500 RPM. That paper included two example applications: (1) a helicopter gearbox, and (2) conditioning monitoring of a railroad track. A second paper, "Improved RotoSense for Rolling Stock: Locomotives and Cars," was presented at the 2018 MFPT conference: it described subsequent improvements to that sensor, in terms of ruggedizing and improving signal quality, to meet requirements of a manufacturer of rolling stock. Included in the description are the rationale, the methods, and the improved results. The sensor described in the first paper was the first known, and is still the only known, to survive, intact, three days of testing at the National Test Track Center in Pueblo, Colorado, including a 10-hour, non-stop, 400-mile test run. Even so, a manufacturer of rolling stock wanted more ruggedizing and better signal quality. This article expands that second paper by including additional details and a new section on improved battery life.
* RotoSense is a Trademark of Ridgetop Group, Inc.

Keywords: *RotoSense; MEMS; helicopter transmission; train axles; wheel hub; vibration; railroad tracks; ruggedization.*
Article history: *Received ; Published .*

1. Introduction

Equipment, such as robotics and gear boxes, that incorporate rotating shafts often need to monitor rotational vibration and shaft speed, as part of broader condition-based maintenance (CBM) systems. Fault detection equipment on drive systems typically use accelerometers mounted on transmission housings to capture, measure, and process vibration signals. The usefulness and flexibility of such detection equipment for applications involving rotating shafts, including pinion and planetary gears, have been limited by cabling, slip-ring approaches, and multiple sensors to obtain monitoring information.

For more complex systems, especially those with poor signal transmission paths, a shaft-mounted, wireless solution based on a micro-electro-mechanical system (MEMS) is needed (see Figure 1) [1] [2] [3] [4].

A prototype solution was designed, developed, and imbedded on a rotating shaft used in helicopter transmissions to capture and measure vibration signals, and then a MEMS version mounted on the wheel hubs of rolling stock was developed.

This article focuses on the methodology and results in ruggedization, improved signal quality, and increased battery life of those solutions.

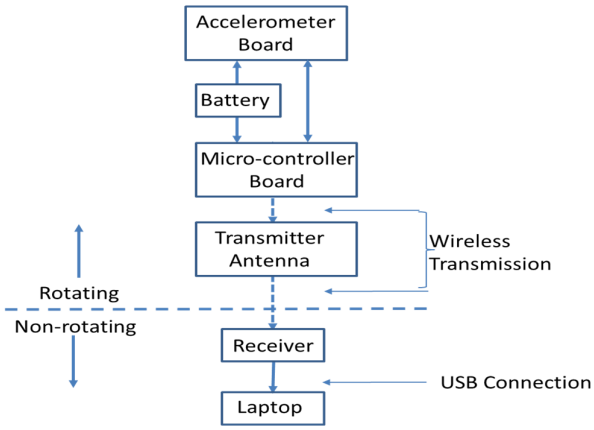

Figure 1. Simple MEMS block diagram [2]

2. Theoretical Background

MEMS-based accelerometers that measure acceleration and force, such as produced by vibration and shock, were used in prototype solutions for the following applications: (1) mounting inside helicopter transmissions and (2) mounting on the hubs of rolling stock of trains to detect features of railroad tracks.

2.1. Helicopter Transmission: Pinion Gear.

A specific application was the spiral-bevel pinion of an OH-58C transmission (see Figure 2). For that application, MEMS Sensing Package was designed and developed to contain Figure 4a microcontroller board, an accelerometer board, and a battery pack mounted in a cylindrical canister (Figure 3 and Figure 4).

A NASA Glenn Research Center, Small Business Innovation Research (SBIR) award led to an experiment in which a tooth on the spiral bevel gear was pre-notched and then the transmission was run to tooth failure. The purpose was to prove the feasibility of shafted-mounted solutions and compare results with those obtained from traditional stationary, housing mounted accelerometer solutions.

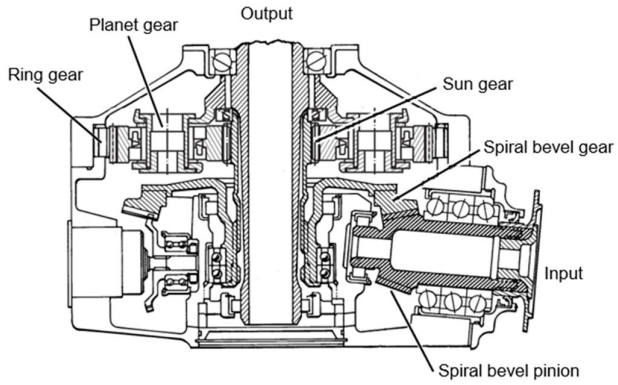

Figure 2. Illustration of an OH-58C transmission

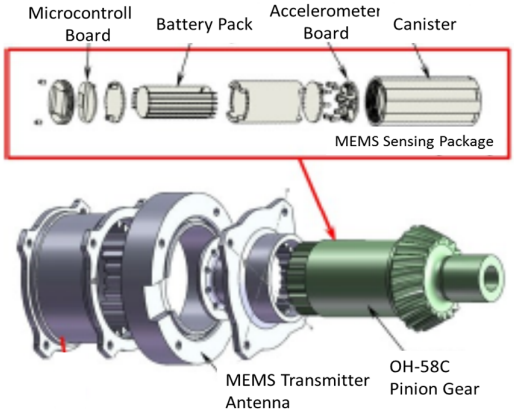

Figure 3. RotoSense mounted on an OH-58C pinion gear

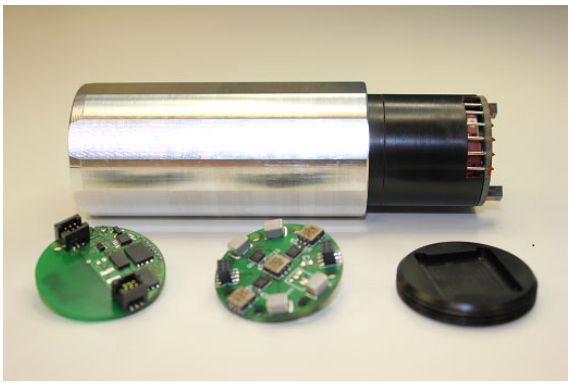

Figure 4. Canister, boards, and end cap

2.2. Wheel Hubs of Rolling Stock

Figure 5 shows the physical adaptation of the MEMS-based sensor for mounting on wheel hubs of the shafts of the trucks of train locomotives and cars. This version of the sensor was designed and developed to prove feasibility for using such sensors to locate and identify anomalies related to railroad tracks.

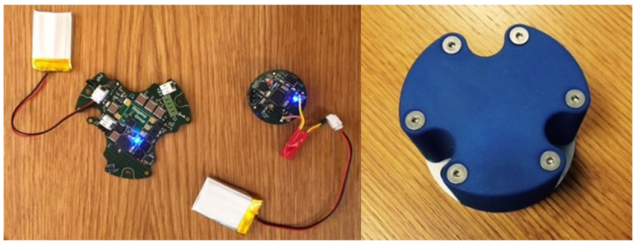

Figure 5. Boards with batteries and housing assembly

Referring to Figure 6, the adapted system for rolling stock applications comprises a MEMs sensor and a gateway to collect data and write data to disk storage as files. The MEMS sensors were mounted on wheels of a train to produce shock data during test runs of a train over a High Tonnage Loop (HTL) test track (TT) to process the data, identify high-force events (HFEs), and locate the position on the HTL TT where HFEs occurred. The purpose was to demonstrate/validate an ability to support focused inspection of tracks to identify and locate anomalies requiring monitoring and service [2].

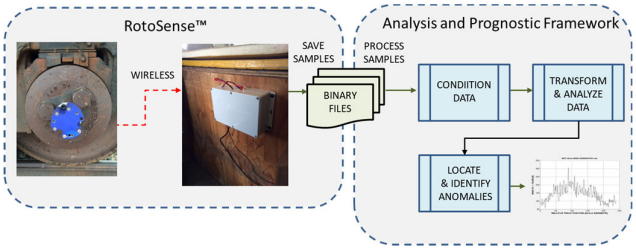

Figure 6. Block diagram of a rolling-stock sensor system

2.3. Initial Results: Shaft-mounted, beveled-pinion gear

Triaxle-shaft-mounted MEMS sensors, RotoSense, were installed on pre-notched OH-58C spiral-bevel pinion gears and endurance tests at NASA's Glenn Research Center were performed and run to tooth fracture failure: the notch was extended at run time = 51.9 hours and widened at run time = 106 hours: see Figure 7.

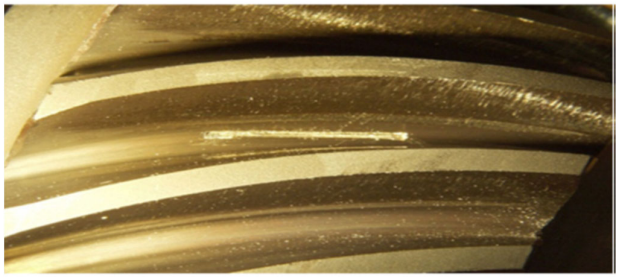

Figure 7. Final notching of the gear tooth

The sensors performed well, lasted the entire test, and all MEMS accelerometers gave an indication of failure at the end of the test. The MEMS systems performed as well, if not better than, the existing stationary accelerometers mounted on the gear box housing with regards to gear tooth fault detection (Figure 8).

Figure 8. Failed gear – fractured tooth

For both the MEMS sensors and stationary sensors, the fault detection time was not much sooner than the actual tooth fracture time. The MEMS sensor spectrum data showed large first order shaft frequency sidebands due to the measurement rotating frame of reference. The method of constructing a pseudo tach signal from periodic characteristics of the vibration data was successful in deriving time-synchronous-average (TSA) signals (Figure 9) without an actual tach: the method proved to be an effective way to improve fault detection for the MEMS [1].

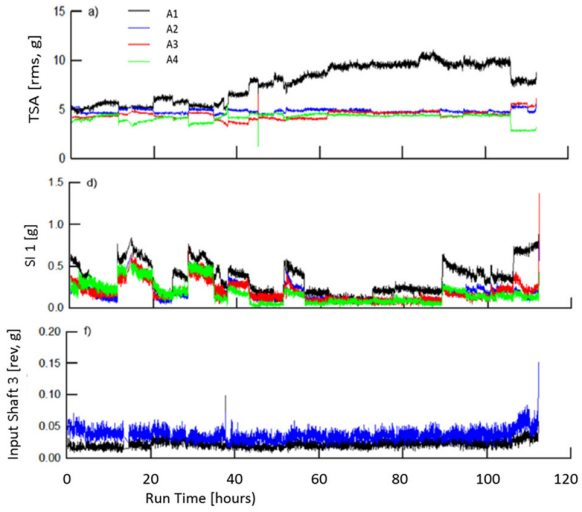

Figure 9. Example data: detection, condition indicators

2.4. Initial Results: Hub-mounted, freight car of a train

The configuration for train applications includes RotoSense, a MEMS sensor, supporting firmware and software to support collecting, wireless transmitting of data to a gateway, and saving data in binary files. The assemblies are mounted to the wheel hubs to rotate with the axle so any anomalies in the wheels or track can be detected (see Figure 10).

Figure 10: RotoSense mounted on a wheel hub

2.4.1. MEMS Configuration

The MEMS is configured as a three-axis accelerometer with 57mV/g sensitivity with a 161 Hz sampling rate: sensor was mounted concentrically on each end of a freight car axle and also on a locomotive axle of a train, as shown back in Figure 10.

2.4.2. Test Train

A test train at the National Test Track Center at Pueblo, Colorado, comprised three (3) locomotives and 110 freight cars and was run on a high-tonnage loop (HTL) test track (TT) used for research under heavy axle-loads to test track-component reliability, wear, and fatigue.

2.4.3. Test Track

The HTL track length is 2.7 miles divided into test sections that generally correspond to tangents, spirals, curves, and turnouts that are populated with features and test sections, as seen in Figure 11.

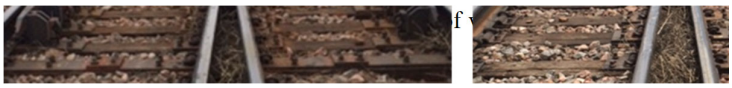

Figure 12 and Figure 13. Fast-train operation is restricted to a maximum 40 miles per hour.

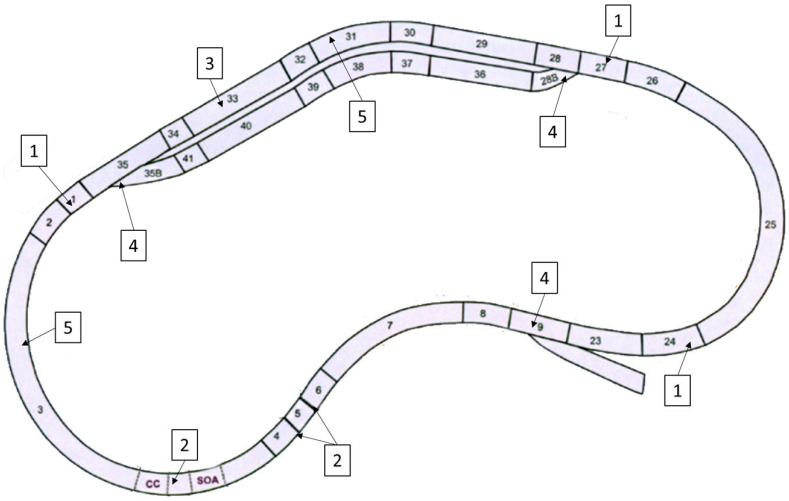

Figure 11. Layout of the Heavy Tonnage Loop Test Track**.**

Table 1. Physical Features of the HTL TT – refer back to Figure 11

1. Lubricator	2. Steel Bridge	3. Crib Ties and Fasteners
4. 405, 407 or 408 turnout and frog or switch	5. Thermite or Overlay Welds	6. Concrete Bridge

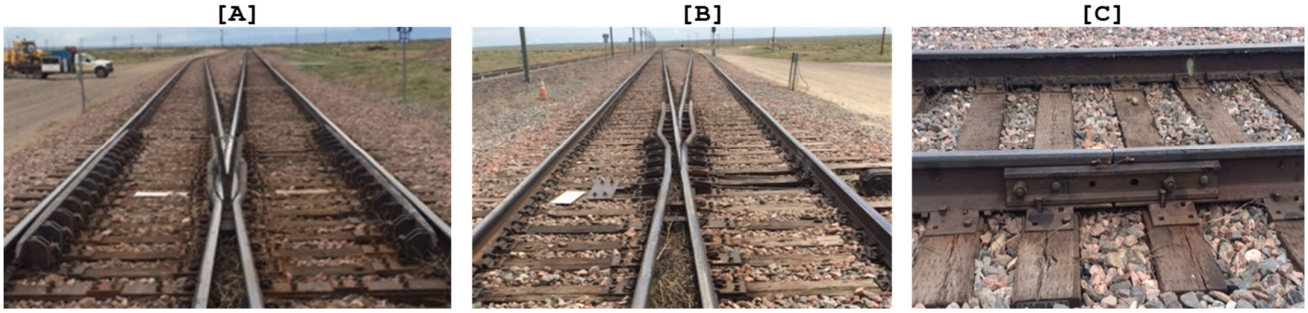

Figure 12. Turnout and frog, switch left [A] and switch Right [B]; steel bridge [C].

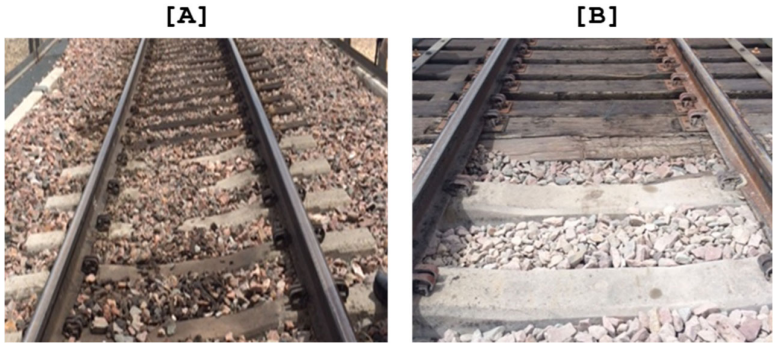

Figure 13: Concrete bridges [A]; crib ties, top of [B]; concrete bridges, bottom of [B].

Train Movement—The train was auto-controlled to run 15 laps per hour: 4 minutes per lap and 38,640 samples per lap. Four test runs were started on four days in 2015: May 11 – May 14.

Table 2 summarizes the May 14 test run from 2000 to 0632 the next morning: 10 hours, 32 minutes and over 4 million sets of six-byte data. The train started to move about 30 minutes after the sensors were turned on: the train was moved to the test track and two laps of test conditioning were run. After that, the train was kept at a constant speed of 15 laps per hour (4-minute laps).

Table 2. Summarization of the test run started on May 14, 2015

Description			**Comments**
Train	3 locomotives 110 cars		6,780' long (1.3 miles). Hopper car lengths, coupler to coupler, range from ~58.5 to 60.5 feet: used 60-foot length.
Build	92 minutes		2000 start; 2132 completed build
Run	540 minutes	132 laps	2132: started test conditioning run (TCR)
	17 minutes	2 laps	2149: completed TCR
	518 minutes	129 laps	2149 – 0627: testing
	5 minutes	1 lap	0632: end of test
Wheel 1	20645 files		
Wheel 4	20565 files		

2.4.4. Test Data

Data was collected and buffered for each axis at a sampling rate of 161 Hz and the buffered data was transmitted to a collection hub and saved in output files about once every 1.11 seconds. The data was analyzed, nominal values determined for zero-force conditions, and transformed into +/- values with respect to zero-force.

2.4.5. Data Analysis

Data analysis was hampered by the loss of Global Positioning Data (GPS) caused by a broken antenna. Consequently, raw data

(see Figure 14) was analyzed by binning the data in terms of magnitude (xy-plane, the z-plane, and both planes) and relative laps (see Figure 15), examining the peaks, and comparing those peaks to features of the test track: pattern matching. We successfully proved that, even without GPS, we were able to synchronize the data to the start of the test track and then locate those features that could be located: as seen indicated in Figure 16 and Table 3.

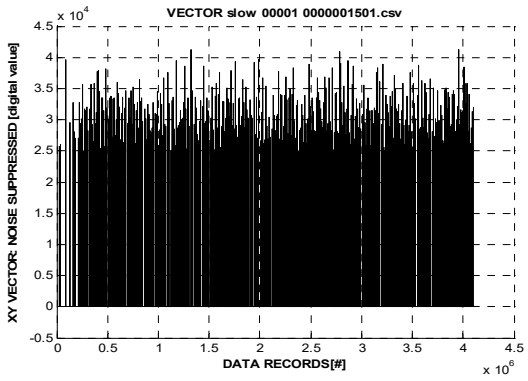

Figure 14. Raw data, xy-plane

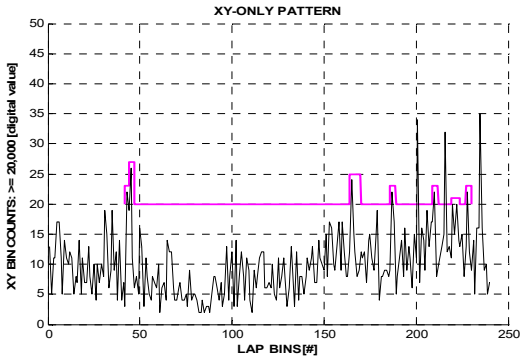

Figure 15. Binned data, xy-plane, by lap-bin number

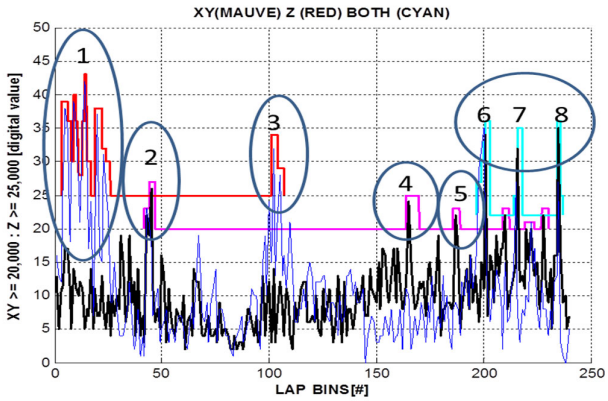

Figure 16. Data and identified features -see Table 3 for (1) through (8) association to feature and location

Table 3. Test track description and detection evaluation

Track Sections	Feature Sections	TT ID	Track Feature	Detection Evaluation	
				XY-vector	Z-vector
1 – 3		S1	Lubricator	ND	ND
4 – 5		S2			
6 - 62	5-26	S3	Repair/overlay welds		Yes **(1)**
	30-40	S3	Concrete bridge	maybe	maybe
	42-46	S3	Concrete bridge	maybe	Yes **(2)**
63 – 66		S4	Steel bridges	ND	ND
67 – 69		S5	Bridge deflection	ND	ND
70 – 73		S6	Steel bridges	ND	ND
74 – 92		S7	Rail performance	ND	ND
93 – 97		S8	Fiber optic cable	ND	ND
98 – 108		S9	405 turnout/frog		Yes **(3)**
109 - 117		S23	405 turnout/frog		Yes **(3)**
118 – 125		S24	Lubricator	ND	ND
126 – 163		S25	TPO, Tie and fastener, performance	Yes **(4)**	No
164 – 170		S26			
171 – 175		S27	Lubricator	ND	ND
176 – 180		S28	Turn out, steering switch, foundation	Yes **(5)**	
181 – 193		S29	LTM Tests	ND	ND
194 – 198		S30			
199 – 208		S31	FRA: Rail-seat deterioration, Thermite welds	Yes **(6)**	Yes **(6)**
209 – 212		S32			
213 – 225		S33	Crib ties	Yes **(7)**	Yes **(7)**
226 – 229		S34			
230 - 240		S35	407 turnout/frog	Yes **(8)**	Yes **(8)**

Note: ND means Not Detectable.

3. Methodology: Ruggedization, Signal Quality, and Battery Life

Subsequently, a manufacturer of rolling stock obtained sensor units and software and performed additional testing and evaluation. The units were found deficient because of the following: (1) physical failure at high-force testing of up to 100 g vibration and shock leading to board flexing and subsequent solder joint failures and battery displacement; (2) inaccurate vibrational readings caused by flexing of the printed circuit boards.

Operational concerns were reported in the following areas: (1) setting up communications between the Sentinel Gateway and Laptop; (2) setting up communications between RotoSense sensor and Sentinel Gateway; (3) sending commands to the RotoSense sensor; and (4) setting a synchronized time on a RotoSense sensor.

The following solution approaches were employed to address the issues and concerns: (1) employ potting; (2) reposition the PCB board and the battery; (3) improve the quality of the built assembly to ensure an ability to withstand stresses and flexing due to high-g vibration and shock; and (4) operational design changes to reduce power consumption and thereby improve battery life.

Quality improvements included inspections and procedures regarding use, assembly, and testing. In addition to hardware and software solutions, documentation improvements were made.

Final testing of the improved MEMS-based sensor, see Figure 17, was performed at the National Technical Systems (NTS) test facilities in Tempe, Arizona and at Ridgetop Group laboratories in Tucson, Arizona.

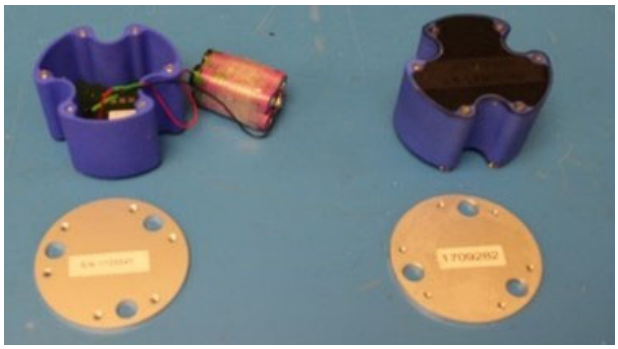

Figure 17. Original (left) and improved (right) sensors

3.1. Epoxy-based Potting

An epoxy-based potting was employed: (1) prevented battery displacement; (2) PCB protection from internal vibration and shock forces; (3) increased accuracy in sensor readings; and reduction of additional internal forces. Experiments were performed on sensor units with no potting, partial potting, and full potting. Partial and full potting addressed battery displacement, but partial potting did not fully address board flexing: full potting yielded the best results: zero defects related to shock and vibration occurred during initial and final testing conducted at Ridgetop Group and at NTS.

3.2. Component Repositioning

Experiments were performed using variations of component placement: the highest quality signals were obtained using the component placement shown in Figure 18.

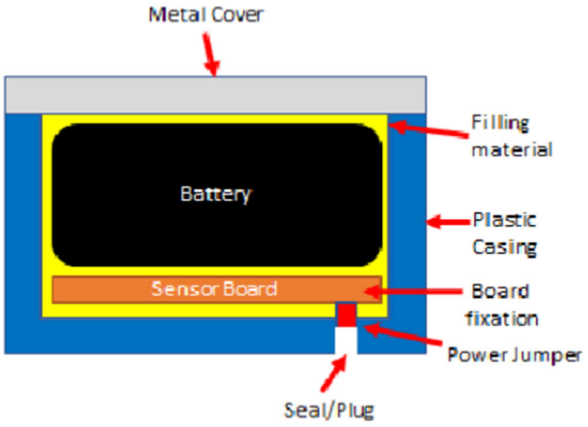

Figure 18. Component placement diagram

3.3. Software and Firmware Improvement

Supporting software updates include an updated file structure for more flexible control of future parameter changes.

Firmware updates include the following:

1. Updated sensor-gateway communications
2. Updated gateway firmware to reduce timeouts
3. Sensor firmware, functional improvements:
   - Ability to change sensor node address
   - Ability to change the computer IP address for which the data is transmitted to
   - Set time on sensors
   - Read sensor temperature
   - Read radio frequency
   - Improved the wireless speed capabilities from 5.5KB/S to 11KB/S.

3.4. Documentation Improvement

The documentation was improved as follows:

1. Improved description of software commands
2. How to change sampling rates
3. How to change node addresses
4. Improved description of use and operation:
   - Procedure to turn off the firewall
   - Memory map functions
   - Operating as an administrator (Admin)

3.5. Operational Changes to Reduce Power Consumption

Power consumption was reduced to increase battery life as follows:

1. Wireless transmission was accomplished using both standard WiFi and Zigbee implementations. Each offers its own advantages. Zigbee uses less power to transmit data, but has a more limited distance. WiFi has a greater range, but consumes more power.
2. Another method to reduce power consumption and increase battery life is the development of software and firmware to dynamically support the following usage modes:
    a. Burst: high-sample rates – 1 kHz to 100 kHz
    b. Streaming: actively sampling and transmitting data at < 1 kHz
    c. Standby (default): actively waiting for a command – default mode
    d. Sleep: periodic sampling of accelerometer with no data storage or transmission when acceleration below defined threshold
    e. Deep sleep: sensor is turned off after a 'no vibration' period of 3 to 12 minutes – dependent on which add-on version is obtained
3. A third method was to redesign and reimplement sub-circuit stages, such the oscillator, voltage regulation, and dividers, to reduce power consumption.

4. Data Collection and Analyses at NTS and Ridgetop Group

Test plans were updated from one to three types of vibration test: (1) fixed frequencies, (2) sweep frequency, and (3) pulse (shock). Testing included tests performed at NTS in June of 2017.

4.1. NTS Testing

4.1.1. Fixed Vibration Frequencies

Three vibration frequencies at seven levels of force defined and tested: Table 4. The sequences were run at four sampling rates: 160 s/s, 250 s/s, 500 s/s, and 1000 s/s.

Table 4. Fixed vibration frequency

Vibration Frequency: Force
Dwell @ 50 Hz: 5g, 10g, 20, 30g, 50g, 70g, 100g
Dwell @ 100 Hz: 5g, 10g, 20, 30g, 50g, 70g, 100g
Dwell @ 250 Hz: 5g, 10g, 20, 30g, 50g, 70g, 100g

4.1.2. Sweep Vibration Frequency

The sweep frequency as defined as 10 Hz to 500 Hz at two different levels of force: 10g and 40g. The sequences were run at the defined four sampling rates.

4.1.3. Pulse Vibration (Shock)

The pulse was defined as a six-millisecond, positive half-sine wave repeated five times at the six different magnitudes of force used for fixed-frequency testing. The sequence was repeated for each of four different sampling rates.

4.2. Ridgetop Development and Testing

Ridgetop design and development engineers, in parallel with preparation and support for NTS-based testing undertook

5. Discussion and Results

5.1. Ruggedization

No physical damage or anomalies were found during and after the testing regime at NTS. At no time was there any loss of signal.

5.2. Improved Signal Quality

After potting and repositioning of components, the signal quality is significantly improved as seen in Figure 19 through Figure 22.

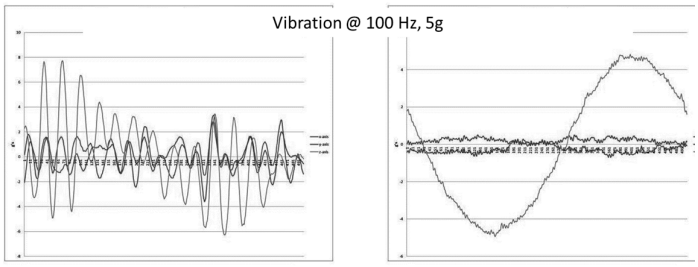

Figure 19. Vibration @ 100 Hz, 5g – before (left) and after (right) repositioning and potting

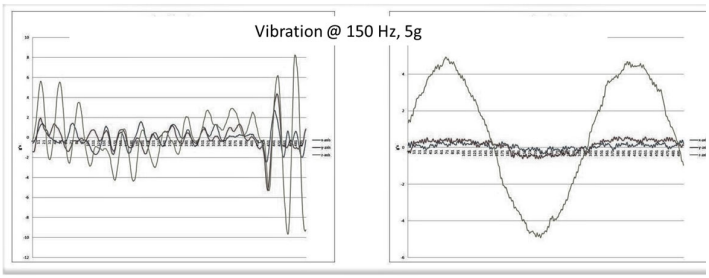

Figure 20. Vibration @ 150 Hz, 5g – before (left) and after (right) repositioning and potting

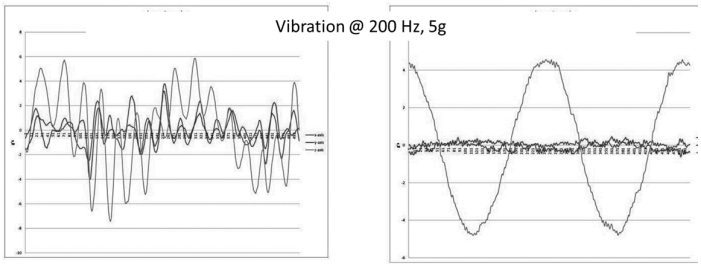

Figure 21. Vibration @ 200 Hz, 5g – before (left) and after (right) repositioning and potting

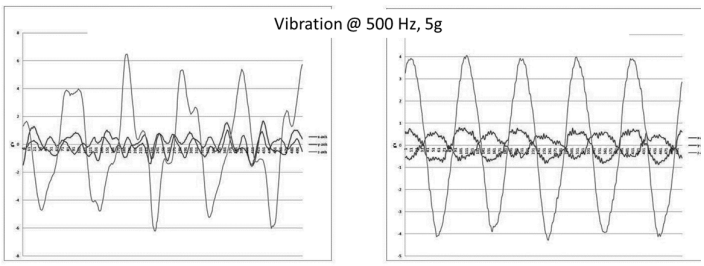

Figure 22. Vibration @ 500 Hz, 5g – before (left) and after (right) repositioning and potting

5.2.1. Reduced Harmonic Distortion and Noise, More Accurate Amplitude Measurements

The output signals from the MEMS-based sensor after repositioning and potting of the boards and battery pack no longer exhibit extreme harmonic distortion and noise; the amplitudes more accurately reflect the magnitude of the vibration force; and the bandwidth has been improved from 4-6 Kb/s to 20-22 Kb/s.

Further improvements in signal quality have been made: primarily through improvements in configuring the ground planes, signal paths, and voltage references.

5.2.2. Improved Gateway

A new version of the Gateway for helicopter use is significantly more rugged: (1) it uses super strong Vicor power supply, that went through extensive power cycle testing on the Apache helicopter; and (2) all internal components are compact, soldered to a carrier board, and/or immobilized.

The new Gateway is compatible with IoT sensors that can communicate through a Wi-Fi connection: at speeds up to 300 MB/s.

5.3. Decreased Power – Increased Battery Life

The operational power consumption has been reduced from the levels at the time of the test runs at the NTTC (2015) to those listed in Table 5.

Table 5. Power Usage (9600 mAh battery)

Usage Mode	2015	2018
OFF	0	0
Deep Sleep	N/A	< 0.001 mA
Sleep	N/A	< 4.0 mA
Standby	45 – 55 mA	< 22 mA
Streaming	40 – 60 mA	< 25 mA
Burst	45 – 75 mA	< 70 mA sampling < 25 mA data transfer

6. Conclusions

Two versions of MEMS-bases sensors were designed and developed: one version for use in gear boxes of helicopters and the other version for hub mounting on axles of rolling stock. Each version of the sensors, their application, and their testing and results were described and the results evaluated: both versions functioned and operated successfully.

Subsequently, it was discovered the version for rolling stock was not rugged enough to pass 100 g vibration testing, and that level of testing was a customer required. After analysis and research, that version of the sensor was ruggedized by repositioning and potting of the components: the boards and the battery pack. The ruggedized version of the sensor was tested at the National Technical Systems at various regimes: fixed frequency, sweep frequency, and pulse mode vibration at various frequencies and levels of force - no physical failure or anomalies occurred.

Improvement in signal quality (level of harmonic distortion) and the accuracy of measured force were verified by comparing signals from non-ruggedized sensors to those from ruggedized sensors. In addition to ruggedization, improvements were made to the hardware to increase sensor bandwidth and to improve the Gateway with respect to ruggedness, to IoT compatibility, and to communication speeds. Hardware design changes in grounding and signal paths were made to further reduce noise.

The software, firmware, and documentation were updated to increase communication, to reduce timeouts, and to increase functionality and usability.

We achieved a significant decrease in power consumption and a corresponding increase in average battery life. We anticipate further improvements in the future, especially with regards to further reducing power consumption; and we are investigating the feasibility of and approaches to energy harvesting and rechargeable methods to achieve further improvements in extending battery life: enabling design changes have already been developed.

Plans are to apply the potting approach to increase the ruggedization of the helicopter version of the sensor. That version has already been improved by increasing the sensor bandwidth, making the Gateway more rugged, and improving Gateway communications.

Acknowledgments

The authors thank Naval Air, Naval Sea, U.S. Army, U.S. Air Force, and NASA research centers for their support and funding of multiple projects that led to the design and development of the prototype solutions and the results described and shown in this paper.

7. References

1. Lewicki, D.G., Lambert, N.A., and Wagoner, R.S., (2015) "Evaluation of MEMS-Based Wireless Accelerometer Sensors in Detecting Gear Tooth Faults in Helicopter Transmissions," NASA/TM-2015-218722.
2. Hofmeister, J.P., Goodman, D., and Wagoner, R. (2016), "Accurate Vibration and Speed Measurement on Rotating Shafts Using MEMS and IoT Single Wireless Triaxle Sensor," Conference of the Society for Machine Failure Prevention Technology, Dayton, OH, 24-26 May, 2016.
3. Hofmeister, J.P., Pena, W., Wagoner, R., and Nielsen, M., (2017) "Improved RotoSense™ for Rolling Stock: Locomotives and Cars," Conference of the Society for Machine Failure Prevention Technology, Virginia Beach, VA, 16-18 May, 2017.
4. Lindstrom, M., (2018) "What's Wrong with My Piezoelectric Accelerometer?" PCB-TN-30-0418, MTS Systems Corporation, PCB Piezotronics, Depew, NY, April 2018.